Petroleum 5 (2019) 13–29

Contents lists available at ScienceDirect

Petroleum

journal homepage: www.keaipublishing.com/en/journals/petlm

Sweet-spot mapping through formation evaluation and property modelling using data from the Goldwyer Formation of the Barbwire Terrace, Canning Basin

Munther Alshakhs*, Reza Rezaee

Curtin University, Petroleum Engineering Department, 26 Dick Perry Avenue, Kensington, WA, 6152, Australia

ARTICLE INFO

Article history:
Received 13 June 2017
Received in revised form
28 February 2018
Accepted 12 June 2018

Keywords:
Sweet-spot maps
Formation evaluation
Petrophysical modelling

ABSTRACT

The Goldwyer Formation of the Canning Basin has been regarded as a highly prospective shale play. This study assesses the potential prospectivity of this source rock as an unconventional hydrocarbon resource. Considering the sparsity of wells penetrating the Middle Ordovician Goldwyer across the vast under-explored area of the Canning Basin, a basin-wide study of the source rock is not warranted. Goldwyer assessment of the Barbwire Terrace, a subdivision of the Canning Basin, is carried out instead.

This assessment includes the estimation of key shale play properties, such as, total organic carbon, total porosity, water saturation, and brittleness index. Each property was estimated from available well data by testing multiple estimation methods. TOC values were derived from multiple regressions of different well data. A simplified Archie's equation was used to estimate water saturation. Density porosity method was primarily used for total porosity estimations. Sonic data along with density were utilized to estimate brittleness index.

Each property was then modelled across the Goldwyer Formation within the terrace. This provided geostatistical estimates on the propagation of such properties. In order to generate sweet spot maps for the Barbwire Terrace, averaged maps of different properties were combined in a weighted manner. This approach attempts to simplify the complexity of unconventional resource assessment, which therefore has provided a single product evaluating the prospectivity of the Goldwyer as a hydrocarbon resource.

Results have shown that TOC and porosity are mostly the deciding factors for the prospectivity of this source rock, given that their values can be too small where the Goldwyer is deemed non-prospective. Nonetheless, sweet-spot maps show that most prospective zone is the Upper Goldwyer (Goldwyer I), followed by the upper parts of the Lower Goldwyer (Goldwyer III). More specifically, southern flanks of north-western and middle regions of the Barbwire Terrace tend to be more prospective. A stricter approach where cut-off values were applied for each property showed that sweet-spot maps are only prospective in the southern flanks of the middle Barbwire Terrace of Goldwyer I.

1. Introduction

The Canning Basin is a broad intracratonic rift basin. It is the largest sedimentary basin in Western Australia where it occupies a massive area of more than 595,000 km^2. About one third of the area of the Canning Basin is offshore with water depths that can get as high as 1000 m. The onshore part of the basin is bounded by the Pilbara and Musgrave Blocks in the south and the Precambrian Kimberley Block in the north. An arch of Upper Proterozoic sediments define the eastern boundary of the Canning Basin with the Amadeus Basin, Fig. 1 [1,2]. The onshore part of the basin covers a

* Corresponding author.
E-mail addresses: munther.alshakhs@postgrad.curtin.edu.au, munther@outlook.com (M. Alshakhs), R.Rezaee@curtin.edu.au (R. Rezaee).

Peer review under responsibility of Southwest Petroleum University.

Production and Hosting by Elsevier on behalf of KeAi

https://doi.org/10.1016/j.petlm.2018.06.003

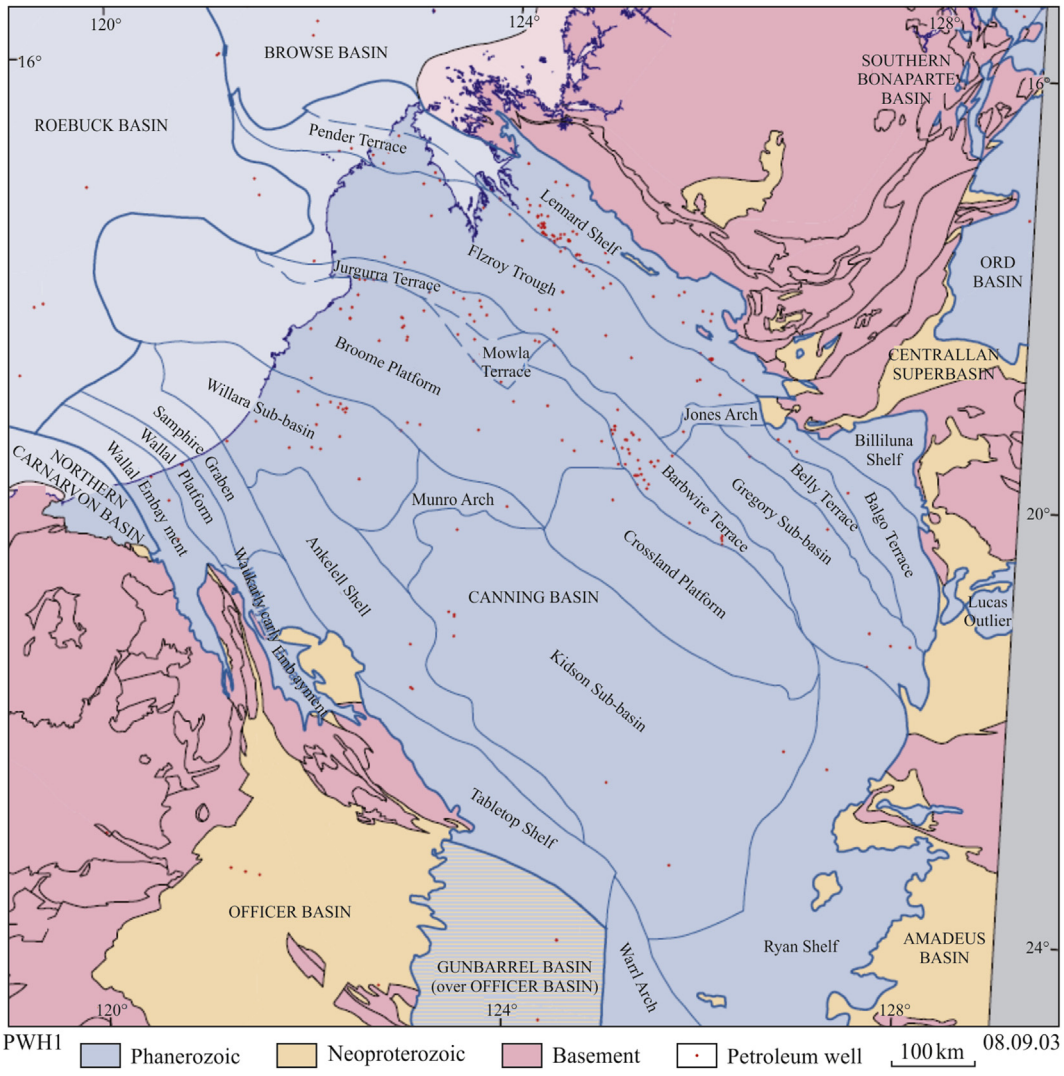

Fig. 1. Boundaries and subdivisions of the Canning Basin (Cadman et al., 1993).

distance of about 800 km from north to south, and 950 km from east to west. It has an area of about 430,000 km^2 [3].

The underexplored Canning Basin has increasing unconventional resource potential. The Goldwyer Formation is considered to be one of the most prominent source rocks in the basin [2]. The average thickness of the Goldwyer Formation is about 400 m and predominantly consists of carbonate and mudstone. Different lithological build ups and distributions occur across the basin [4]. Given the vast area of the scarcely explored Canning Basin, an assessment of the Goldwyer Formation across the whole basin is not feasible. A focused look into the Goldwyer Formation of the Barbwire Terrace was carried out instead.

The Goldwyer Formation was deposited in an open marine shelf conditions. The facies of the formation indicate alternating depths of water column. Some parts of the section indicate quiet subtidal shelf or lagoon conditions, and other parts suggest higher energy shoal and intertidal conditions. In general, the Goldwyer Formation goes through two broad deepening and shallowing trends [4].

Based on the source rock lithofacies, the Goldwyer Formation can be divided into different zones. One common division identifies three zones; upper shale (Goldwyer I), middle limestone (Goldwyer II), and lower shale (Goldwyer III). The middle limestone zone can vary in development in different part of the basin. Much greater carbonate content can be observed in the Goldwyer section of platforms and terraces of the basin [4,5]. This study utilizes the same three-zone division.

Although various studies have been published on different conventional prospects in the Canning Basin, limited research has provided adequate assessment of the Goldwyer Formation as a potentially prospective shale play. Maturity data is commonly mapped for the Goldwyer Formation to provide an understanding of the maturity distribution across the basin [6]. The US Energy Information Adminstration EIA [2] published a regional assessment of the Goldwyer Formation in the Canning Basin making it potentially one of the most prospective Ordovician shale plays in the world [2]. Similarly, Triche and Bahar [5] provided a more detailed assessment of the shale gas volumetrics of the Goldwyer Formation mainly using data of thermal maturity, kerogen type, hydrocarbon generation potential, rock mineralogy, and fluid analyses. This study, however, carries out a more detailed formation evaluation of the Goldwyer and incorporates sweet spot mapping of key properties the define the reservoir and completion quality of the shale play. We evaluated major properties that define the prospectivity of most shale plays; maturity, TOC, porosity, saturation and brittleness. Such an evaluation across the basin requires an adequate well distribution, and hence, this study was limited to the Barbwire

Terrace, a subdivision of the Canning Basin.

2. Maturity of the Goldwyer

Maturity data from Rock-Eval pyrolysis were analyzed from five wells in the Barbwire Terrace. Cross-plots of T_{max} and HI (hydrogen index), Fig. 2, suggest the Goldwyer Formation, in this terrace, is in the early to peak oil generation window. This is generally in agreement with the maturity model provided by Brown et al. [6]. All available Rock-Eval data can be accessed individually in the Western Australia Petroleum and Geothermal Information Management System (WAPIMS) website [7].

3. Property estimation methods

3.1. Total organic carbon TOC

This property is a key factor in determining the prospectivity of any shale play. It significantly influences hydrocarbon production [8]. TOC is traditionally measured in a laboratory from core data, sidewall plugs, and cuttings. Such measurements are relatively more accurate methods in TOC estimation. However, it provides non-continuous measurements of the source rock section as it has limited samples and is usually associated with higher costs and longer measurement time. To overcome these limitations, different continuous wireline data are often utilized to derive TOC.

Petrophysical properties of kerogen and TOC vary greatly than those of the hosting source rock matrix. The presence of TOC generally leads to higher gamma-ray (higher uranium content), lower density, higher resistivity, and slower sonic [9,10]. Consequently, different methods and approaches were introduced to estimate TOC from well log data.

Schmoker method is a widely used approach, and it estimates TOC from formation density logs. In general, a shale mineral matrix density has an average of about 2.7 g/cc whereas the density of organic matter is within the range of 1.2–1.4 g/cc. Thus, the presence of organic carbon will highly influence the formation bulk density and hence TOC can be calculated from density log when other factors for density variation are taken into consideration [11].

Passey et al. [12] is another method that was proposed as an advanced technique to estimate TOC compared to the simple estimation from density or gamma-ray logs [13]. The *ΔlogR* technique of Passey et al. [12] includes estimating TOC from three methods; sonic/resistivity, neutron/resistivity, and density/resistivity logs. The approach evolves around the log separation that occurs between the resistivity and the other logs, due to the presence of organic matter [10].

Another common approach in TOC estimation is data regression. Given there is sufficient TOC measurements, single and multivariate regressions are plotted to derive TOC from various wireline log data. This was also widely utilized and validated in this study.

3.2. Fluid saturation

Estimating the resistivity values of water-filled porous rocks is the key step of estimating the water, oil, and gas saturations of a given formation. Accordingly, Archie [14] introduced such a relationship using sandstone samples.

$$R_o = FR_w \tag{1}$$

Where R_o is the resistivity of the sand when all pores are filled with water, R_w is the brine resistivity and F is the formation resistivity factor.

F is generally a function of the type of the formation and its characteristics. Changes in permeability and porosity of the formation will influence the value of F. Hence, the formation resistivity factor and porosity have the following relationship:

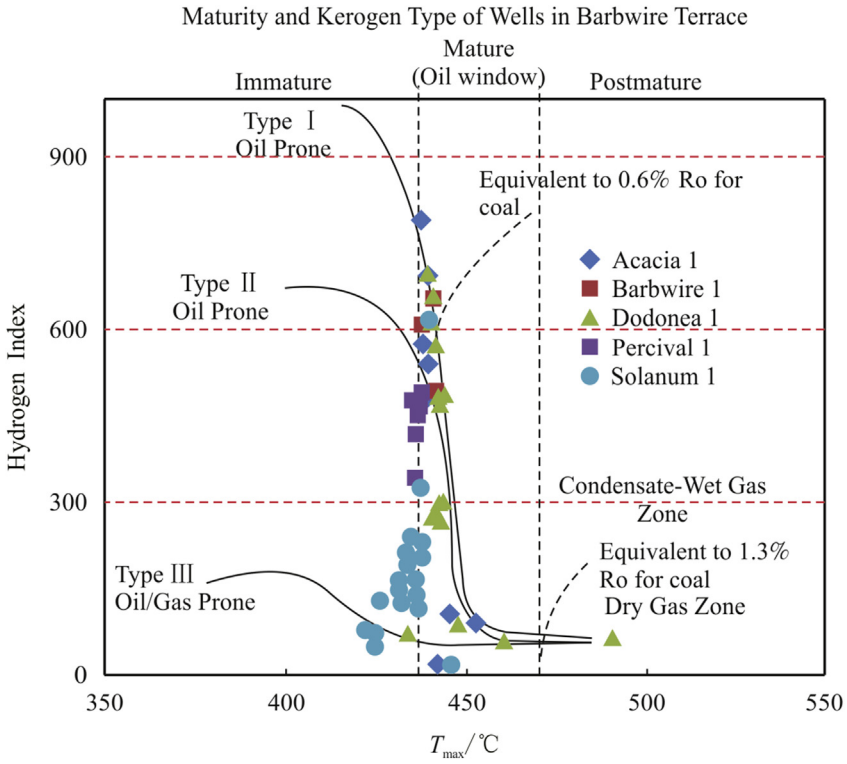

Fig. 2. Maturation of the Goldwyer Formation in the Barbwire Terrace appear to be in the early to peak oil generation window.

$$F = \frac{1}{\varnothing^m} \tag{2}$$

By combining Eq. (1) and Eq. (2).

$$R_o = \frac{R_w}{\varnothing^m} \tag{3}$$

Where Φ is porosity and m is the cementation exponent which is the slope of the line representing the relationship. For consolidated/unconsolidated sandstones, m is generally in the range from 1.3 to 2.0.

In the case of the presence of oil or gas in the formation, Archie [14] derived an equation to estimate the water saturation (S_w).

$$S_w = \sqrt[n]{\frac{R_o}{R_t}} \tag{4}$$

Substituting Eq. (3) into Eq. (4) gives.

$$S_w = \sqrt[n]{\frac{R_w}{\varnothing^m R_t}} \tag{5}$$

Where R_w is the brine resistivity, R_t is the log resistivity and n is the saturation exponent, whose value is ~2 for consolidated sandstones.

It is very difficult to estimate R_w from shales. They are not water producing formations, and shale salinity tends to be highly variable and hence substituting a value for R_w might be unreliable [15,16]. Archie's method assumes one value for water resistivity and does not account for different electrical contributions from different types of water partially filling the pores of shale. Therefore, this simplified model can be a source of error when used for shales as we can't account for the different electrical contributions coming from free water and clay-bound water in shale source formations [17].

In a conventional sense, electrical current flows in the rock using the formation water as pathways. In shales, the abundance of clay and the associated clay-bound water increase these pathways and hence increase the ease of the electric current flow. This would lead to a reduction in the formation factor and, consequently, a reduction in m (cementation exponent) to a value smaller than 2 [15,18,19].

Eq. (4) is a simplified form of Archie's method and can be used to quantify water saturation of a shale interval. R_o is the resistivity of a lean shale in the interval, where it represents a shale rock with water-filled pores [15]. R_t is simply the deep resistivity log along that shale interval. Saturation exponent n can be given the value of 1.7 as proposed by Luffel and Guidry [20] as it provides a good match to water saturation derived from core data. With the water saturation estimated, the hydrocarbon saturation S_h can be calculated using Eq. (6) [17]:

$$S_h = 1 - S_w \tag{6}$$

3.3. Porosity

There are different techniques used to measure porosity and permeability in petroleum shales in a laboratory. Sample crushing was one technique introduced by Luffel and Guidry [20] to increase surface area. Porosity estimations of this method require bulk density, dry matrix density, bulk volume, and grain volume measurements. However, removal of capillary and clay bound water, pore access difficulties to gas, adsorption, sample size, crushing methods, crushed sample weight, and effect of pore pressure and overburden on microfractures are all different factors affecting the validity of those measurements [16].

There are other direct porosity measurements of shales but they are still affected by some of the factors mentioned earlier. Those measurements include nuclear magnetic resonance NMR and high-pressure mercury injection capillary pressure MICP. NMR total porosities are validated with those of core measurements and they both agree for a wide range shale plays [21]. MICP measurements were typically done for shales to assess seal capacity [22]. Nonetheless, this method has recently become popular for estimating porosity for shale plays [23].

Shale gas reservoirs have typically low porosities. They usually have a range of 3–10%. Reliable porosity estimations from petrophysical logs in shale gas is an important tool for economic shale evaluation. Different methods were developed for porosity measurements in the conventional reservoirs. However, porosity in shale reservoirs has more complexity in the estimation of variable mineralogy, kerogen low-density and distribution, fluid types, and complex nano-to micropore volumes [16,24].

Total porosity is commonly derived from density log for a given formation. Eq. (7) shows the density porosity (DPHI) relationship [15].

$$\varnothing_{density} = \frac{(\rho_{ma} - \rho_b) + \rho_b\left(w_{TOC} - \rho_{ma}\frac{w_{TOC}}{\rho_{TOC}}\right)}{\rho_{ma} + \rho_f} \tag{7}$$

$\varnothing_{density}$ = density porosity
ρ_{ma} = matrix density
ρ_b = bulk density
ρ_f = fluid density
w_{TOC} = TOC weight fraction
ρ_{TOC} = kerogen density

Fluid density can be assumed to be 0.5 g/cc for gas (ρ_g) and 0.8 g/cc for oil (ρ_o). However, when considering multiple fluid types in the rock, fluid density in the case of shale gas can be estimated as shown in Eq. (8).

$$\rho_f = \rho_g(1 - S_w) + \rho_w S_w \tag{8}$$

ρ_w = water density.

Total porosity can also be derived from sonic data, giving what is known as sonic porosity (SPHI). A different measurement is neutron log which is a downhole log that measures porosity (NPHI). In fact, it is a direct measurement of hydrogen in the formation. Since hydrogen is typically abundant in pore spaces which are filled with water, oil, or gas, hydrogen measurement provides a direct indication of porosity. In shales, however, the relationship is not quite straight forward as hydrogen occurs in multiple other places, like in clay minerals, organic matter, and water/hydrocarbon in the formation [15].

This entails that NPHI reading can increase due to an increase of clay minerals, or it can decrease due to the increase of gas (gas has lower HI). It is also noted that NPHI generally decreases with the increase of the thermal maturity of shale gas. Thus, NPHI reading in shale can suggest misleading interpretation if analyzed independently. Alternatively, analysis of all available logs, such as gamma ray, resistivity, and density should provide a better understanding of the behaviour of NPHI log [15].

3.4. Brittleness

It is a measure of the ability for a rock to fracture and is commonly expressed in brittleness index. It is a function of multiple and complex factors; lithology, mineral composition, TOC, effective stress, reservoir temperature, diagenesis, porosity, thermal maturity, and fluid type [15,25]. According to Jarvie et al. [26], brittleness of a rock is primarily related to mineralogy. For example, the variable contents of quartz, clay, and carbonate in the Barnett Shale result in variable brittleness and hence variable fracture gradient of the source rock interval.

Generally, brittleness in shales increases with the increase of quartz content and decreases (more ductile) with the increase of clay. Carbonate-rich source rocks are usually moderate in brittleness. Thus, brittleness index can be expressed in terms of the mineral composition of a shale rock [15].

$$BI_{mineralogy} = \frac{Quartz}{Quartz + Carbonates + Clays} \times 100 \quad (9)$$

$BI_{mineralogy}$ is the brittleness index derived from mineralogy composition.

Those mineralogy compositions can be determined by using different methods; X-ray powder diffraction (XRD), Fourier transform infrared transmission spectroscopy (FTIR), X-ray fluorescence (XRF), energy-dispersive X-ray spectroscopy setting on the scanning electron microscopy (EDS-SEM), or thin section analysis (TS). In general, XRD, FTIR, and XRF are the most common methods of mineral composition analysis in the oil and gas industry [15].

Alternatively, brittleness index can be defined using the geomechanical elastic properties of the source rock. According to Grieser and Bray [27], the elastic properties of Young's modulus and Poisson's ratio are key geomechanical parameters and are used to identify the brittle/ductile intervals of a shale source rock [28].

$$BI_{sonic} = \frac{E_{brittle} + \nu_{brittle}}{2} \times 100 \quad (10)$$

BI_{sonic} is simply the brittleness index estimated from sonic data. $E_{brittle}$ and $\nu_{brittle}$ are the normalized Young's modulus and Poisson's ratio, respectively. Young's Modulus (E), and Poisson's Ratio (ν) can be estimated using the following equations.

$$E = \frac{\rho V_s^2 \left(3V_p^2 - 4V_s^2\right)}{V_p^2 - V_s^2} \quad (11)$$

$$\nu = \frac{V_p^2 - 2V_s^2}{2\left(V_p^2 - V_s^2\right)} \quad (12)$$

A cross-plot of the two parameters (Young's Modulus and Poisson's Ratio) showing brittle and ductile areas can be seen in Fig. 3 [27]. Whenever a hydraulic stimulation is required for commercial production, brittle areas are preferable to frac into as they are prone to instigate a larger and more complex fracture geometry than those of ductile nature. A brittle interval would have high Young's modulus and low Poisson's ratio values [29].

BI_{sonic} approach is dependent on the sonic well data, of both compressional and shear velocities. In many instances, shear velocity is not available in the well data. Therefore, shear wave velocity is typically estimated from compressional wave velocity. Castagna et al. [30] derived an empirical linear relationship between V_s and V_p. This relationship was derived from worldwide data and became known as the mudrock equation or the ARCO mudrock line [15,30,31].

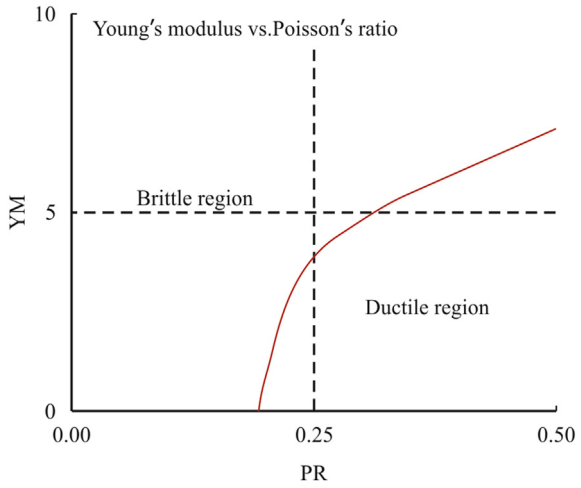

Fig. 3. Young's modulus and Posson's ratio cross-plot indicating brittle and ductile areas (Grieser & Bray, 2007).

$$V_s = 0.862V_p - 1.172 \quad (13)$$

Both V_p and V_s are in km/s.

4. Results

4.1. TOC

4.1.1. Schmoker and ΔlogR methods

TOC was initially estimated using Schmoker and *ΔlogR* approaches. Calculated values of both methods overestimate TOC when validated against TOC measurements from Rock-Eval. This misfit is clearly observed in Fig. 4, a cross-plot between all estimated TOC values of both methods against TOC measurements from Rock-Eval.

It is noteworthy that applying *ΔlogR* method has been suitable in other parts of the Canning Basin. This method has yielded acceptable TOC values in some areas of the Goldwyer Formation.

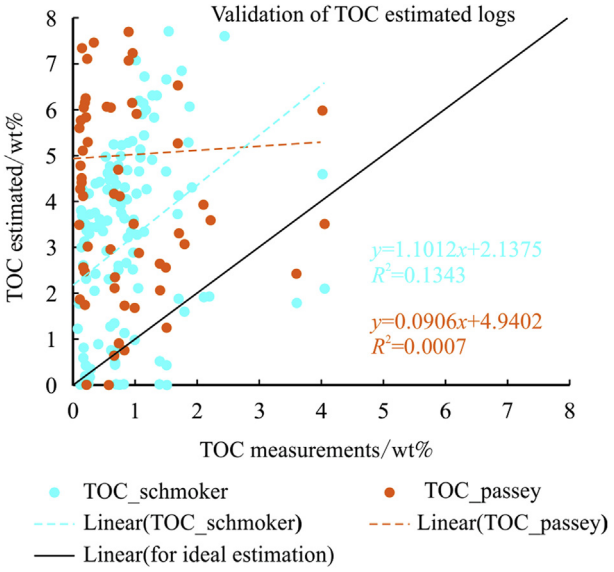

Fig. 4. A cross-plot showing TOC estimated values from all wells in the Barbwire Terrace plotted against TOC measurements. Both methods overestimate TOC.

However, such results mainly require manipulation of different *ΔlogR* parameters that does not necessarily have any scientific basis. For example, available maturity data are not analyzed and interpolated. They are often disregarded and simple manipulation of LOM is carried out instead. This simply entails changing the value of LOM for the whole section until the resultant log agrees the most with the TOC measurements. Such manipulations are not necessarily incorrect approaches, but they are not usually backed by sufficient scientific reasoning. For the purpose of this study, it was decided to prioritize exploring other TOC estimation options over the parameters manipulation of the pre-defined methods to deliver an adequate TOC solution of the Goldwyer Formation in the Barbwire Terrace.

4.1.2. Single and multivariate regressions

Multiple approaches were utilized to test TOC estimation, starting from simple linear regression between Rock-Eval TOC measurements and density (RHOB). Poor correlation was observed from this regression. It was then improved by applying data depth matching of TOC samples coming from cuttings, and removing few data points that were identified as outliers.

Once good correlation of single regression was established, various multiple regressions were tested. Best TOC estimating approach was identified to be the one derived from gamma-ray (GR) and density (RHOB). This conclusion took into account data availability, where such derivation can be applied to most number of wells in the terrace.

For better analysis of the Goldwyer, the formation was divided into three main zones. One TOC equation was derived for each zone from gamma-ray (GR) and density (RHOB).

$$TOC_{zone1} = 0.0076 \cdot GR - 3.165 \cdot RHOB + 7.96 \quad (14)$$

$$TOC_{zone2} = 0.0034 \cdot GR - 2.28 \cdot RHOB + 6.18 \quad (15)$$

$$TOC_{zone3} = 0.0029 \cdot GR - 2.3 \cdot RHOB + 6.09 \quad (16)$$

Where zones 1, 2, and 3 are upper zone (Goldwyer I), middle limestone (Goldwyer II), and lower zone (Goldwyer III) respectively. These equations were applied to all wells in the Barbwire Terrace for TOC estimation. Derived TOC shows lowest estimation in Goldwyer II, where bottom Goldwyer I and top Goldwyer III generally show highest TOC estimation. The resultant TOC values correlate very well with TOC measurements in Fig. 5 and Fig. 6.

4.2. Water saturation (S_w)

Water saturation estimation uses Eq. (4) as a simplified form of Archie's equation to calculate saturation for a prospective source rock. The approach solely depends on resistivity log, and hence, water saturation is estimated for all wells with resistivity logs across the Goldwyer Formation. There are four wells in the Barbwire Terrace with resistivity logs covering the whole Goldwyer interval.

Equation (4) requires an estimate value for the resistivity of a lean shale. Such a value can be estimated from TOC Rock-Eval measurements and resistivity cross plots. However, The variations of water depths during the deposition of the Goldwyer Formation from high energy conditions to quiet subtidal shelf or lagoon as noted by Haines [4], has resulted into alternating facies across the Goldwyer Formation. Lumping those facies altogether and using one R_o value to represent them all would warrant unreliable estimations. Alternatively, the Goldwyer Formation was broken down into different facies using the volume of shale log derived from gamma ray. For example, the facies breakdown of Acacia 2 and the assignment of R_o for each facies is illustrated in Fig. 7.

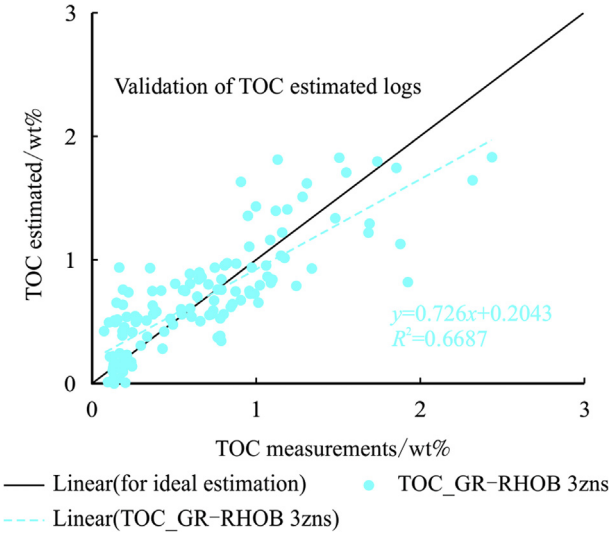

Fig. 5. Estimated TOC values cross-plotted against Rock-Eval TOC measurements. For a perfect TOC estimation, the cross-plot trend line would be overlaying the diagonal solid line, where line slop is one, y-intercept is zero, and R^2 is one.

The limestone intervals that are predominantly in Goldwyer II cannot be considered shaly with volume of shale that is less than 15%. Therefore, a simplified Archie's equation will not yield reliable saturations. A resistivity of a lean shale (R_o) cannot be estimated from a lean non-shale interval. Full Archie's equation should be applied instead (Eq. (5)). Nonetheless, identifying the resistivity of formation water is challenging for non-conventional reservoirs as water samples are very difficult to retrieve and water salinity can be variable across the tight rock interval. Since those sections have very low porosities and with effectively zero TOC, they are expected to be fully saturated with water. Hence, tight limestone intervals with volume shale less than 15% were simply given water saturation of one (fully water saturated). This step was only carried out after mudlog data and all other available hydrocarbon tests indicated no gas/oil traces are present across such intervals.

The saturation exponent n, was given the value 1.7 for shales as proposed by Luffel and Guidry [20]. Consequently, water saturation was calculated for each facies using the corresponding estimated R_o value. Water saturations for individual facies were later combined to form S_w log across the whole Goldwyer. Treating each facies individually has provided more reliable estimations. The estimated S_w logs correspond to TOC changes appropriately (Fig. 8). Water saturation decreases as total organic carbon increases, and vice versa. Additionally, the resultant water saturation values show encouraging values of generally less than 30% across the shaly Goldwyer intervals.

4.3. Total porosity (PHIT)

Total porosity was estimated using density porosity method (Eq. (7)). Porosity values were derived for wells with available density logs across the Goldwyer section in the Barbwire Terrace. Water saturation and TOC information were also utilized for this porosity estimation.

This approach, however, requires assigning values of certain parameters to properly estimate porosity. A value needs to be assigned for the matrix density of the Goldwyer Formation. Available eight-well study of Goldwyer core analysis from WAPIMS

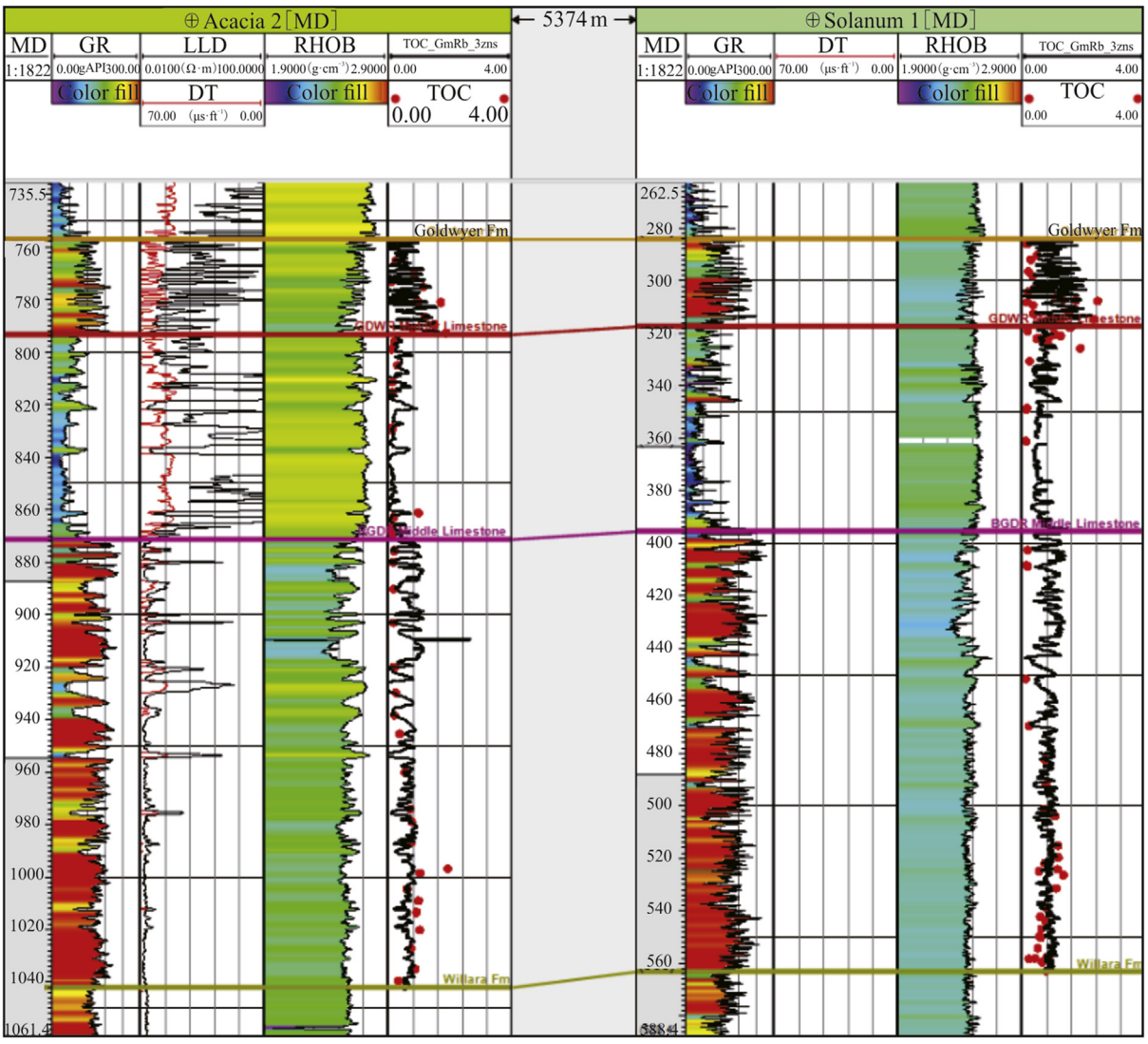

Fig. 6. TOC log derived from gamma-ray and density individually for each Goldwyer zone. Wells Acacia 2 and Solanum 1 are shown as an example.

database indicated that the Goldwyer Formation is limestone-dominated in different parts of the Canning Basin, including the Barbwire Terrace. It has also locally undergone a significant secondary dolomitization. Another study had looked into Goldwyer III core of a well in the Canning Basin and reported an average matrix density of 2.73 g/cc. This value was implemented as the matrix density of the Goldwyer in our density porosity estimation. Water density is 1.1 g/cc, oil density is 0.8 g/cc, and density of kerogen ranges between 1.2 and 1.4 g/cc [32–35]. Density of kerogen ($\rho_{kerogen}$) is sensitive to its maturity. Ward [36] illustrated how we can derive kerogen density from vitrinite reflectance (R_o), Eq. (17) [15,36]. Average T_{max} values of samples of the Goldwyer Formation in the Barbwire Terrace is 435 °C. According to Jarvie et al. [37], this is equivalent to 0.7 $\%R_o$, which results into kerogen density of 1.2 g/cc once calculated from Eq. (17).

$$\rho_{kerogen} = 0.342R_o + 0.972 \quad (17)$$

Similar to the estimation of water saturation, the limestone (non-shaly) intervals that predominantly occur in the Goldwyer II zone, had their porosities calculated differently. Typical limestone matrix density (2.71 g/cc) was used to estimate density porosity, where kerogen density was irrelevant as TOC is effectively zero in these intervals. In theory, density porosity values and neutron porosity readings should be the same in a limestone interval that is fully saturated with water [38,39]. Hence, an average between the two porosities is taken as the total estimated porosity. This approach was applied for all intervals with volume of shale less than 15%.

The resultant total porosity (PHIT) is fairly stable with reasonable values. Porosity is lowest in the Middle Goldwyer Zone (Goldwyer II), which is thought to be the zone of lowest TOC richness and predominantly consists of tight carbonate rock. Porosity estimation generally increases in the other two zones of Upper and Lower Goldwyer (Fig. 9).

4.4. Brittleness index (BI)

Brittleness can be simply described as the measurement of the ability for a rock to fracture. This property is dependent on various rock factors, including mineralogy, porosity, and effective stress. It is generally expressed in terms of brittleness index (BI) which can be calculated by using the geomechanical elastic properties of the shaly source rock, BI_{sonic} (Eq. (10)).

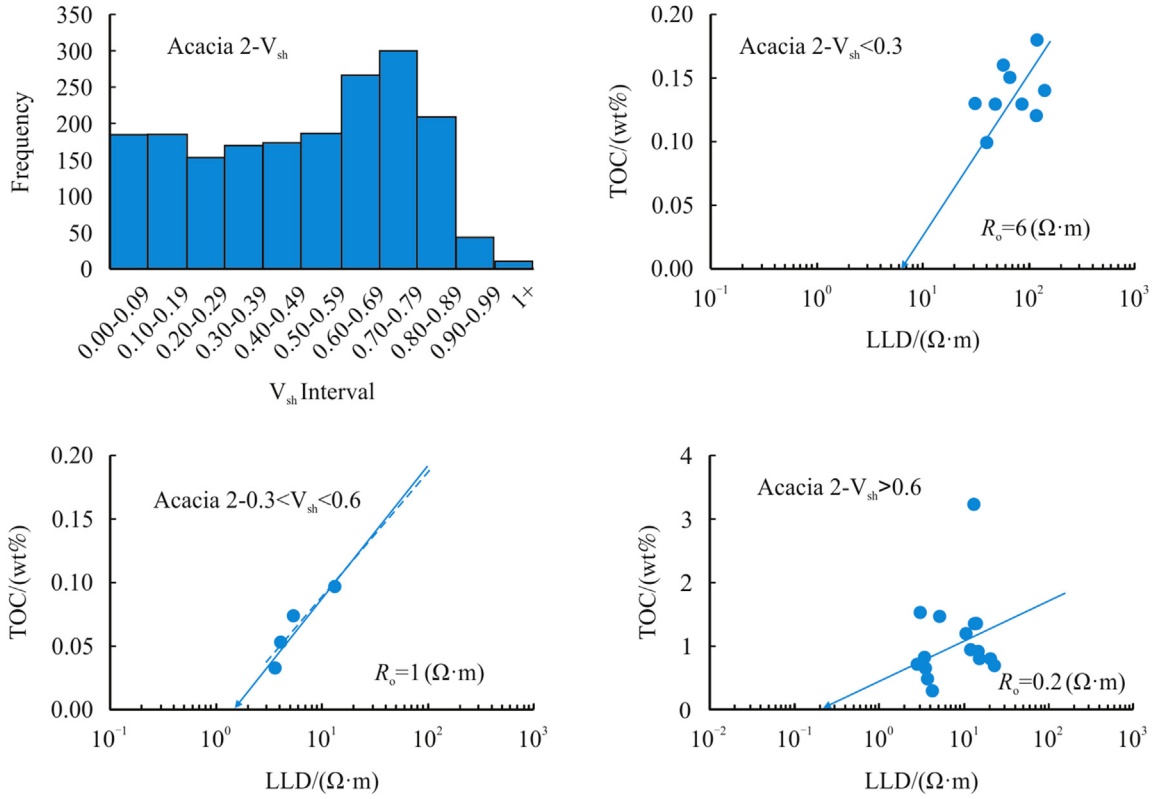

Fig. 7. Graphs show the breakdown of the Goldwyer into three facies using V_{sh} log in Acacia 2. Ro values were then estimated for each facies using the shown cross plots.

Prior to estimating BI_{sonic}, calculating both Young's modulus and Poisson's ratio is required, (Eq. (11)) and (Eq. (12)), respectively. Shear velocity (V_s) data are not available in wells of the Barbwire Terrace. V_s data were therefore derived from the V_p/V_s relationship proposed by Castagna et al. [30] in Eq. (13).

The resultant Young's modulus and Poisson's ratio are then normalized before undergoing the estimation of the brittleness index. The normalization, however, uses minimum and maximum values that are only extracted from parts of the Goldwyer where V_{sh} is 0.5 or greater, to ensure that the normalization process is tailored around the shaly sections of the Goldwyer Formation.

A well section of some key wells in the Barbwire Terrace with BI data is shown in Fig. 10. The middle Goldwyer zone is the most brittle. Lower brittleness index values are observed in the top and lower Goldwyer zones.

5. Analyses of estimated properties

With all four properties estimated (Fig. 11), a better analysis of the Goldwyer Formation in the Barbwire Terrace can be carried out. Original log information is always valuable for formation evaluation. However, porosity, TOC, water saturation, and brittleness are, in this case, key properties for evaluating the prospectivity of the Goldwyer as a shale play.

Derived TOC data across wells in the Barbwire Terrace show lowest values in Goldwyer II. This is expected as this middle zone is known to be lean and mainly consist of tight limestone. Goldwyer I and III, however, contain varying quantities of TOC and certainly appear to be more prospective than Goldwyer II. Zones with highest TOC values can slightly vary from one well to another. Overall TOC values tend to be highest at the bottom of Goldwyer I and top of Goldwyer III. The Goldwyer Formation may have gone through deposition of relatively abundant amounts of organic matter in anoxic conditions, interrupted by the deposition of the middle limestone zone where very limited organic matter had been deposited and preserved. Nevertheless, the TOC values of the Goldwyer Formation in the study area are generally quite low. All TOC measurements and estimated values are less than 2.5%.

The derived properties are often influenced by one another. A clear example is the TOC and porosity logs. They both have similar signatures across the whole Goldwyer section. Density was the main input for the estimation of both properties, which will result in both logs being highly influenced by the same property, and hence some similarities can be observed. However, the porosity of shale plays, in many cases, tends to mimic TOC regardless of the derivation approach. As TOC increases, there is a higher chance of hydrocarbon generation which will be hosted in pore spaces. Furthermore, kerogen-hosted porosity would increase as there is more TOC, and hence more kerogen in the rock. Consequently, a strong agreement between porosity and TOC logs is often regarded to porosity being abundantly hosted in the organic matter. This is often verified by scanning electron microscope (SEM) imaging.

Subsequently, porosity values tend to be highest in the top of Goldwyer III and the bottom of Goldwyer I. Slightly lower porosity appears in the remaining parts of the two zones. The Goldwyer II, however, mainly consists of tight limestone with porosity values close to zero. Density porosity values of the Goldwyer Formation are overall below 10%.

In theory, Water saturation should somewhat be related to TOC as well. An increase in TOC could potentially increase hydrocarbon generation which by definition would decrease water saturation. In general, estimated S_w shows reasonable water saturation quantities across the shaly Goldwyer intervals of values that range around 15–30%. High water saturation values are found in the lean tight carbonate intervals that are predominantly in Goldwyer II and sometimes in Goldwyer III. This was manually edited after

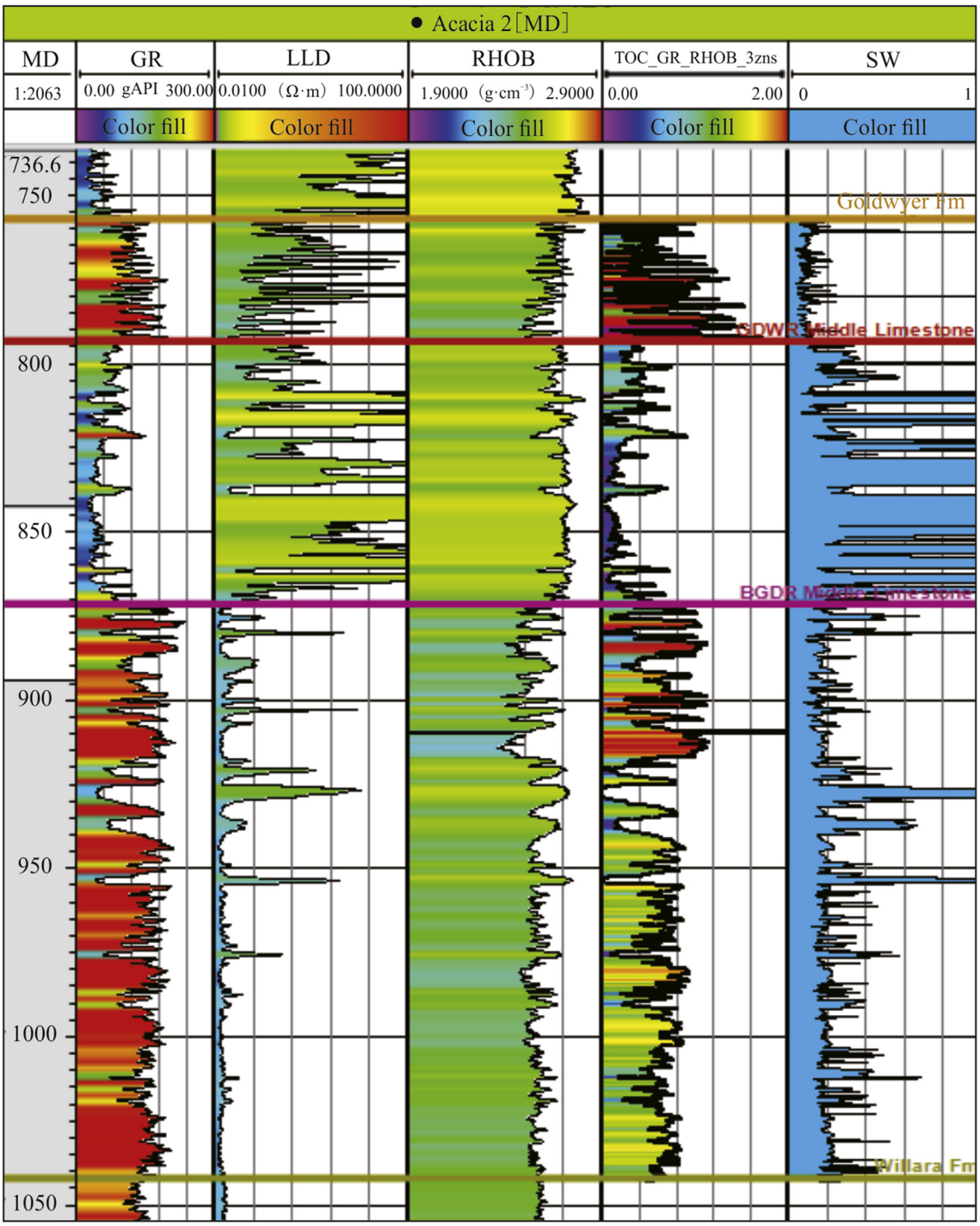

Fig. 8. Water saturation behaviour relative to TOC changes. S_w decreases as TOC increases, and vice versa. Well Acacia 2 is shown here as an example.

confirming the lack of any hydrocarbon traces from mud gases and other hydrocarbon tests across such intervals, as discussed earlier.

Brittleness index estimation was carried out as an attempt to measure the ability of the rock to break. This indicates how the rock would react to hydraulic fracturing process in a well completion stage. The presence of clays and organic matter tends to influence the brittleness index negatively. Such compositions are more lenient to be ductile. On the other hand, the abundance of calcite or silica in the rock commonly lead to a more brittle interval. Shales often would have variable brittleness index based on the change of composition of the shale interval. The Goldwyer Formation is no exception, the low TOC, low porosity, and high calcite content zone of Goldwyer II has the highest brittleness index values of the whole Goldwyer section. In Goldwyer I and III where we have variable compositions and changing amounts of TOC and porosity, brittleness index would be variable accordingly. This does not indicate that wherever there is high TOC, there is ductile rock. TOC is one factor out of many that influence brittleness. Some wells show BI average of about 35% in Goldwyer I and III, where others can go higher than 50% while containing similar amounts of TOC.

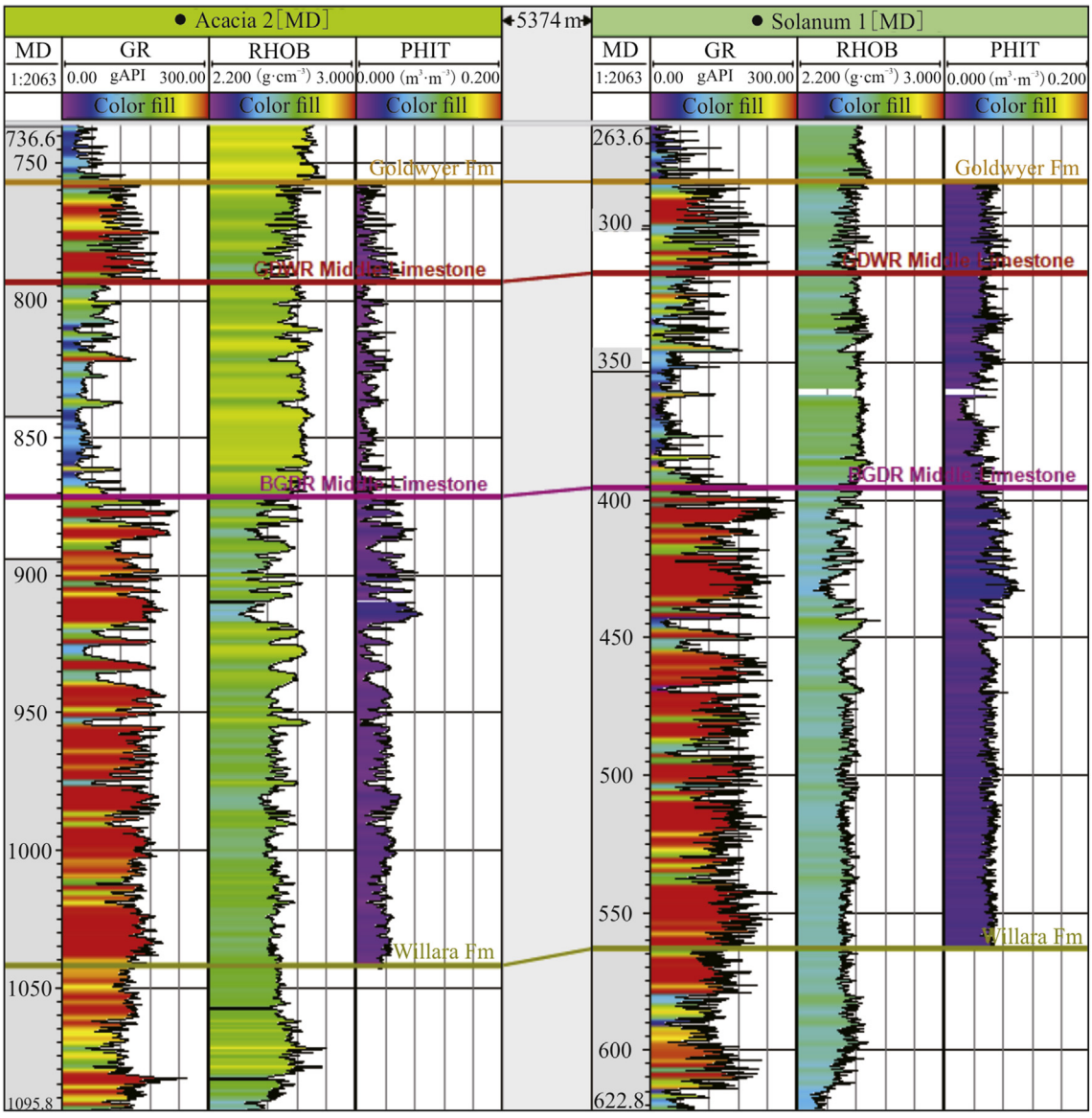

Fig. 9. Estimated total porosity values for Acacia 2 and Solanum 1 as examples of wells in the Barbwire Terrace.

Spiky behaviour and sudden variations in logs can be observed in data of most properties of the Goldwyer. In most cases, such a behaviour suggests a laminated shale. Those laminations represent sudden changes in rock properties resulted by changes of conditions during deposition. Those laminae appear to have relatively low TOC, low porosity, high water saturation, and high brittleness index. This reinforces the concept of cyclic sediments and thin limestone interbeds stated by Haines [4].

The laminae-induced highly variable brittleness in some intervals could act as a geomechanical barrier of hydraulic fracture propagation. Furthermore, intervals with high lamina frequency could also end up producing more water than anticipated. This case emphasizes the significance of well placement and how considering such occurrences along the process can decide how successful a certain well is.

Goldwyer I and III generally show prospective values of different key properties. However, the bottom section of Goldwyer I and the top part of Goldwyer III are optimized shale intervals. They contain the highest TOC and porosity, low water saturations, and adequately high brittleness. The laminations are somewhat minimized in those intervals in some wells but still exist, nonetheless. As a result, laminations could be an occurrence that needs to be analyzed and worked around, once they are confirmed to pose issues in completed future wells in the area.

In most cases, the values of TOC and porosity are in the low-end corresponding to borderline prospective shales. Therefore, the generally low values of the two properties are believed to be the most important factors in deciding the prospectivity of the Goldwyer in the terrace.

6. Property modelling

6.1. Surface generation

Formation surfaces are essential for building any model. In this study, surfaces were generated using well tops data. Those surfaces are the main structural inputs for the property models, which only contains the Goldwyer Formation and assesses property estimation

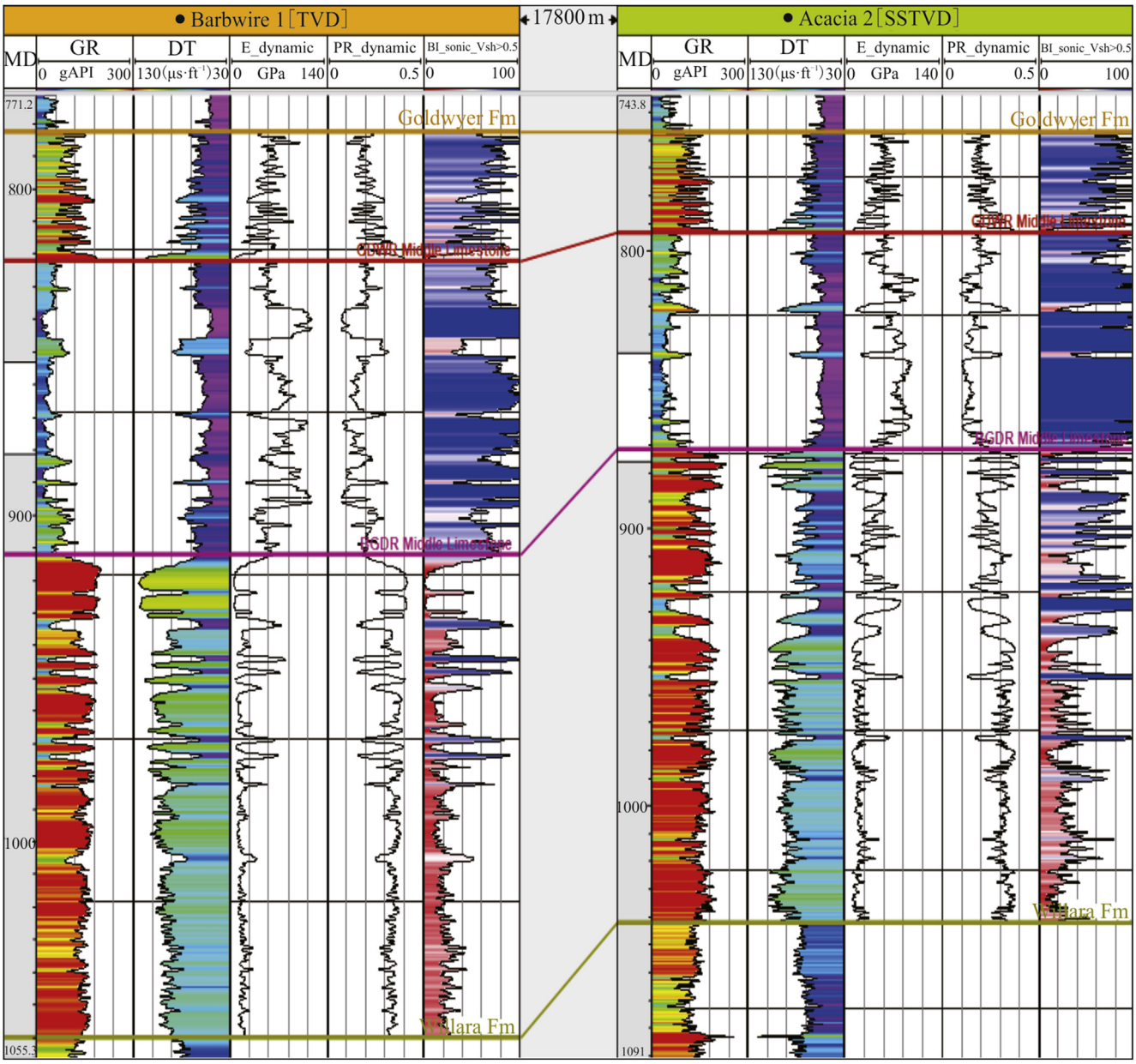

Fig. 10. Brittleness Index derived for some wells in the Barbwire Terrace. Wells Barbwire 1 and Acacia 2 are shown here as an example.

and distribution. Therefore, only surfaces necessary for building the whole Goldwyer section were generated; Goldwyer I, Goldwyer II, Goldwyer III, and Willara (base of Goldwyer Formation).

Given the limited well control and the uneven well distribution across the Barbwire Terrace, a considerable amount of extrapolation is undertaken in some parts of the terrace. In such case, surface intersections and pinch outs can commonly occur in the surface modellng. To resolve such issues, pseudo-well-tops are sometimes utilized in areas that lack well control. Such data points help guide the algorithm to generate conformable and geologically sound surfaces. Needless to mention, this step can be destructive in building any model if data was assigned prematurely. Careful placement of formation tops and zone thicknesses is crucial step in this process. Hence, a thorough geological understanding of the formation extension and structure is necessary. In our study, this approach has proven to be most effective in providing best geologically estimated surfaces of the Goldwyer zone in the Barbwire Terrace.

6.2. Model generation

With the surfaces of interest have been generated, building a structural model is now feasible. This is a simple model that is only considering the Goldwyer section. The grid increment of the model was set to be 500 × 500 m. This is the lateral cell size of both x and y directions.

More information can be added to the structural model, such as, fault surfaces and layering. No fault information has been incorporated in this study. However, subzones were added to the model. The model has three main zones as mentioned earlier. Goldwyer I (*Zone 1*) was divided into two subzones. The two subzones are identical in thickness. Goldwyer II (*Zone 2*) was split into three subzones of identical thicknesses. Whereas *Zone 3* was divided into six subzones that are also identical in thickness (Fig. 12).

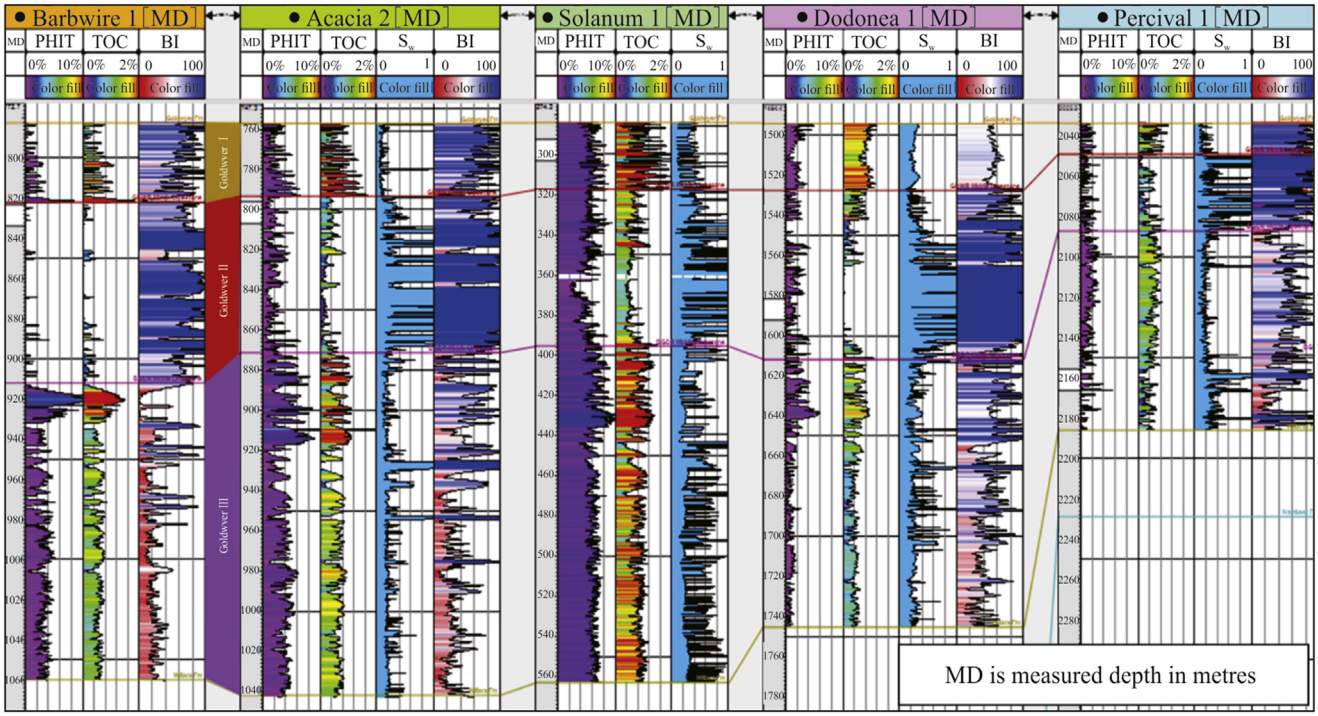

Fig. 11. Well correlation of Barbwire Terrace key wells; Barbwire 1, Acacia 2, Solanum 1, Dodonea 1 and Percival 1 showing all four estimated properties, which are (from left to right) total porosity (PHIT), TOC, water saturations (Sw), and brittleness index (BI).

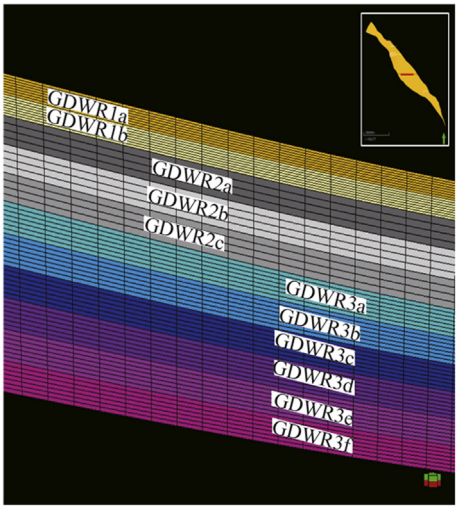

Fig. 12. A cross section of the geometrical model illustrating the sub-zoning of the model and the vertical resolution.

The number of subzones for each zone was determined by the resultant average thickness of the subzones. The average thickness of each subzone is almost the same (~20 m). This makes assessment of different prospective subzones of the Goldwyer more reliable, as average maps are calculated and compared from all subzones.

Layering was then defined into the model. It represents the model's vertical resolution. Looking into facies changes and well log behaviour is important to decide the appropriate vertical resolution for the model. Rock profiles with minimal change in characteristics can afford to have coarse resolution. Similarly, Goldwyer II Zone has consistent lithology with minimum change in rock properties and therefore was assigned a vertical resolution of about 5 m in average. Goldwyer I & II zones, however, have more alternating facies and variable well log characteristics. Subsequently, they were assigned a higher vertical resolution of about 3 m in average.

6.3. Petrophysical modelling

Once all geometrical aspects of the model are finalized, property modelling is carried out. The first step of this process is upscaling well logs. TOC, PHIT, S_w, and BI logs are upscaled to the model's vertical resolution. This is achieved by estimating a single property value for each vertical resolution block through arithmetic averaging method. Then a 3D petrophysical model for each property in the Barbwire Terrace was calculated using a Gaussian Random Function Simulations. The simulations used the default isotropic lateral distribution with a spherical variogram type. Since there is no evidence to assume large difference between neighbouring samples [40], nugget value was kept to the small default of 1×10^{-4} (Fig. 13).

Sieving through all petrophysical models and evaluating areas of high and low potential is time consuming and often impractical. For the purpose of this study, property average maps were generated for each subzone in the 3D model. This is a common practice to simplify the assessment of the prospectivity estimated by the model.

6.4. Sweet-spot mapping

A practical approach of combining different analytical information for a certain shale play is sweet-spot mapping. The process aims to simplify the prospectivity evaluation of a shale play, where property modelling is often involved. It is utilized to combine whatever data or models deemed necessary to provide a critical assessment of the unconventional resource. This could include a wide range of information, such as petrophysical models, geophysical attributes, structural information, geomechanical data,

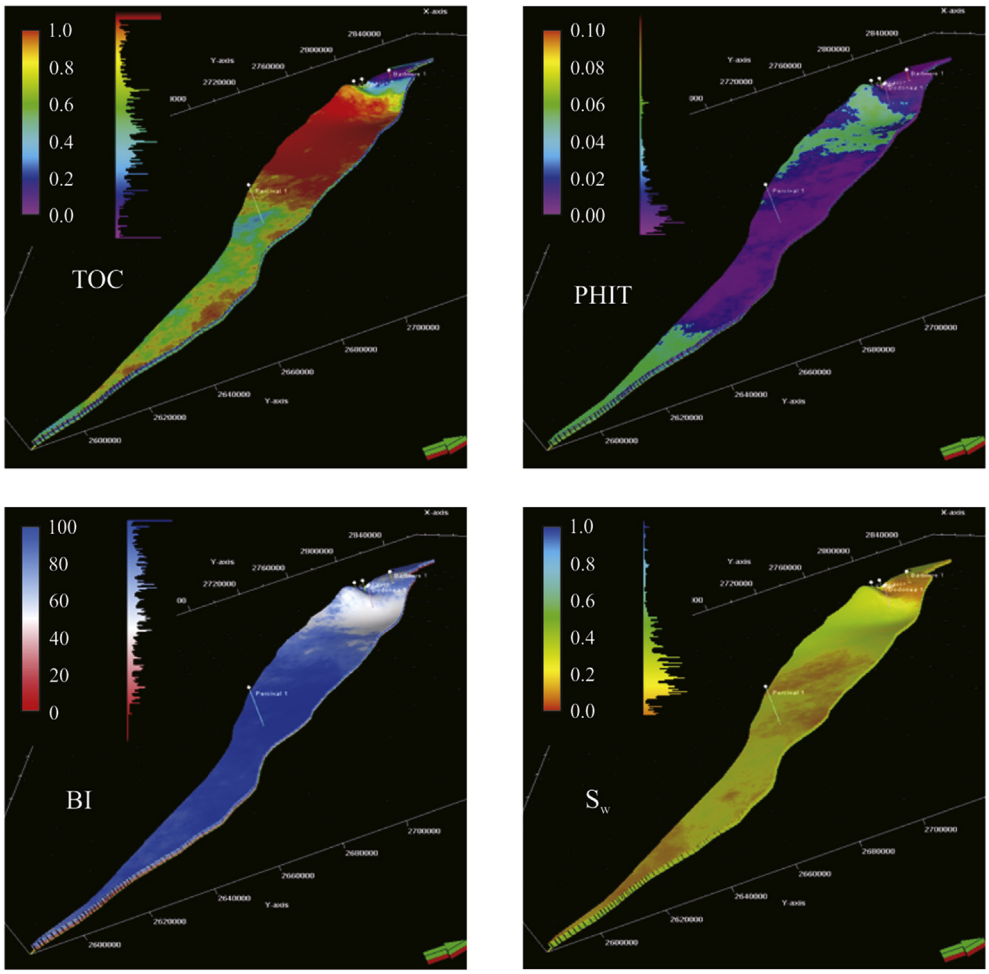

Fig. 13. Property models for the Goldwyer Formation, Barbwire Terrace.

and production history.

A main objective of this study is to look into the formation evaluation aspects of the Goldwyer Formation. Consequently, the associated sweet-spot mapping is combining the four key properties estimated earlier in the study; TOC, PHIT, S_w, and BI. For such a combination to be valid, all properties are normalized so that adding different petrophysical models can be meaningful. However, normalizing property average maps should not be done independently. Same normalization parameters of each property are applied to all subzone average maps. This is essential to keep each property comparable across the different zones and subzones.

Before combining the different properties together, analyzing each one individually is required to see what the resultant values would indicate. Higher values of TOC, PHIT, and BI all suggest higher prospectivity of the Goldwyer Formation. However, higher S_w values suggest the opposite. In order to make such property combination meaningful, we replace S_w with S_h (Eq. (6)), so that higher values of any property suggest higher prospectivity of the shale and vice versa.

Thickness information was integrated into all generated petrophysical models as part of the model's main structure. In the form of average property maps, however, thickness and all other structural information are eliminated. There is an average thickness of each map, which was fixed to be ~20 m for every subzone, but no actual thickness data across the map. Since thickness plays an important factor in the prospectivity of the shale play, where thicker prospective shale is favourable and more prospective than a thin one, thickness was also incorporated in the calculation of the sweet-spot maps in addition to the other four estimated properties. Thickness isochore maps for each subzone were normalized to be implemented in the sweet-spot map estimation. Similar to the other properties, the normalization process is not done independently for each subzone isochore, same parameters are applied to all thickness maps across the Goldwyer.

Properties are added in a weighted manner, each shale play has some properties that are more important than others. For example, a shale play could have relatively high TOC values all across the formation, but the abundance of clay could deem the source rock non-prospective for adequate hydraulic stimulation and sufficient production. This example would entitle clay content or brittleness index to have a higher weight than TOC in generating sweet-spot maps.

In the case of the Barbwire Terrace, however, brittleness index and hydrocarbon saturation of the shaly sections of the Goldwyer Formation suggest overall consistent rock quality. On the other hand, TOC and PHIT values tend to be too low in some areas where they are considered non-prospective. As a result, BI and S_h average maps were given relatively lower weights of 0.18 each, thickness was given the same weight as well. TOC and PHIT were given weights of 0.23 each, the sum of all utilized weights must be one. The resultant sweet-spot map of each subzone can be expressed in Eq. (18).

$$Sweet\ Spot\ Map = TOC(0.23) + PHIT(0.23) + S_h(0.18) + BI(0.18) + Thk(0.18) \quad (18)$$

Where *TOC*, *PHIT*, S_h, and *BI* are all normalized property average maps of each subzone. *Thk* is the normalized thickness of each subzone. Based on the aforementioned maturity information, the Barbwire Terrace is generally considered to be mature in the oil generation window and hence no maturity information was incorporated in the sweet-spot approach.

The resultant maps represent the prospectivity of the Goldwyer expressed in the four combined properties plus thickness. The values of the maps range between 0 and 1, where 0 is least prospective and 1 is the highest estimated prospectivity of Goldwyer. In further discussions, these values will be referred to as *prospective values*.

6.5. Sweet-spot analyses

Eleven sweet-spot maps were generated, one for each subzone in the Goldwyer. An overview of all sweet-spot maps can be seen in Fig. 14. The least prospective section of the model is Goldwyer II

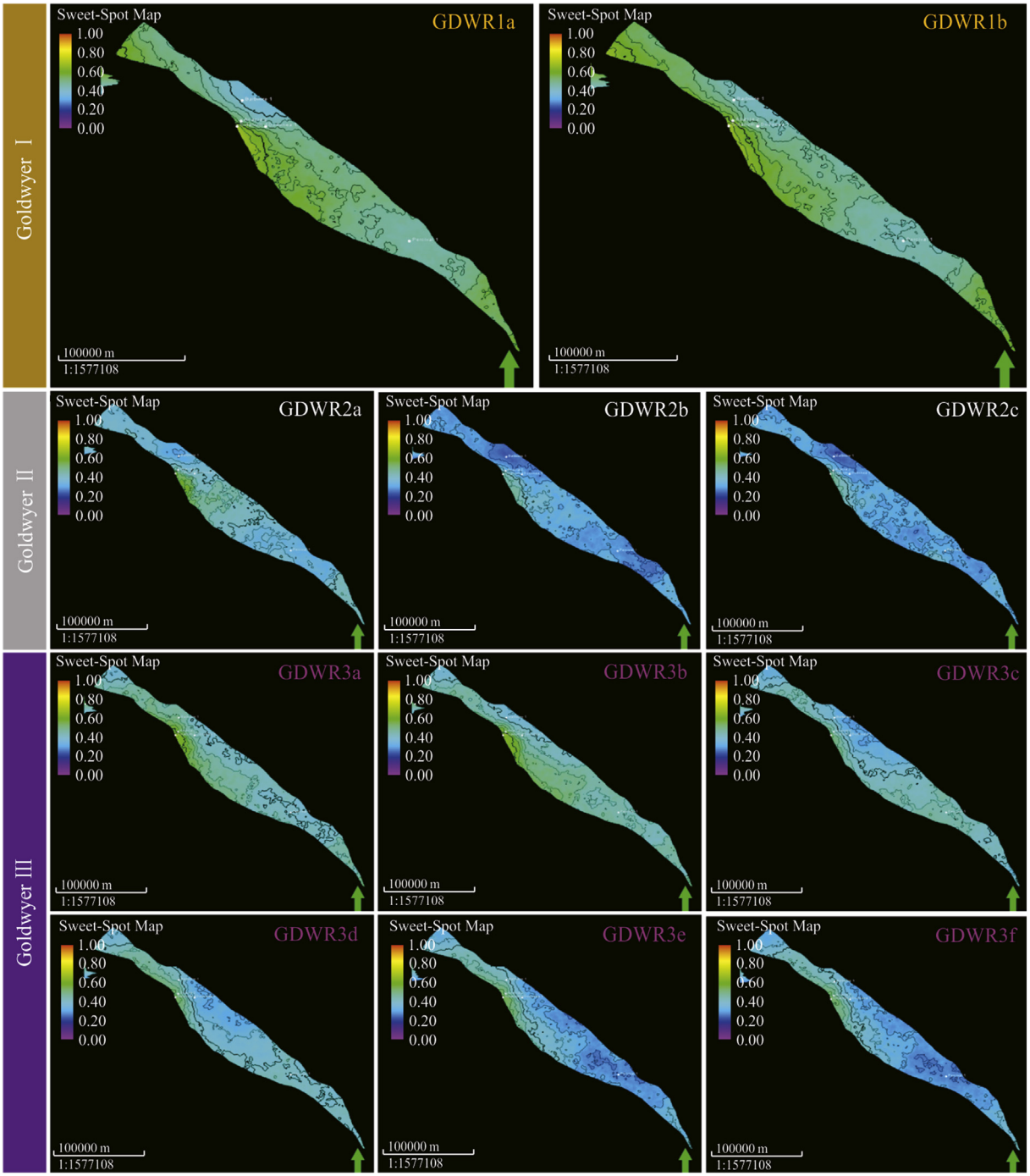

Fig. 14. Sweet-spot maps for all subzones of the Goldwyer Formation model, Barbwire Terrace.

(Zone 2). This is expected as the middle Goldwyer is known to be predominantly lean carbonate zone. Subzones in Goldwyer III have varying potential, upper subzones seem to be more prospective. This is especially highlighted in the top two subzones; GDWR3a and GDWR3b. However, the most prospective zone in the model is Goldwyer I, where both subzones appear to be relatively more prospective than any other subzone in the model. Nonetheless, the deeper GDWR1b shows more prospectivity than the shallower GDWR1a subzone.

A common characteristic of sweet-spot maps of all subzones is that prospective values tend to generally improve around the areas of Acacia 2, and Solanum 1 wells. Those wells have relatively higher TOC and PHIT values. Other common high prospective values are those that appear at the north-western end of the terrace and are mainly caused by the anticipated thickness increase interpreted from the surface generation model.

One sweet-spot map representing all zones of the Goldwyer in the Barbwire Terrace was also produced (Fig. 15). It attempts to provide a single solution for the Goldwyer assessment process and it gives much broader overall analyses than that of the more focused eleven-subzone sweet-spot maps. The resultant map shows higher prospective values in the middle and northern parts of the terrace than the southern portion. More specifically, the southern flanks of northern and middle areas are more prospective than others. This is rather consistent with the trend we have seen from different maps of individual subzones.

It is noteworthy that this specific sweet-spot mapping approach can be misleading in the case of drastic value increases or decreases. For example, a relatively very high increase in thickness can indicate an area to be quite prospective even if it had too low TOC content for a sufficient hydrocarbon production. Therefore, sweet-spot maps can be alternatively estimated after applying cut-off values for each property. Those cut-offs eliminate all areas where each property is deemed non-prospective for a successful shale and the resultant sweet-spot maps only show areas where all properties have prospective overlaps.

Assigning cut-off values is somewhat subjective. Nevertheless, the TOC cut-off was given to be 1%, where all areas of TOC averages less than 1% were eliminated. Similarly, porosity was given a cut-off value of 3%. Whereas general cut-off values for brittleness index and hydrocarbon saturations were considered to be 50% and 55%, respectively. No cut-off value was applied for thickness but it was analyzed for the resultant areas. In this case, the resultant average maps are not normalized but instead converted to volume fractions by dividing each map by its maximum value. Similar to the previous approach, the volume fraction estimations are not done independently for each subzone, a same maximum value is applied to all maps across the Goldwyer. This is, again, significant to keep each property comparable across the different subzones. Sweet-spot maps are then calculated using Eq. (18), where TOC, PHIT, S_h, BI, and Thk are all volume fraction maps instead of normalized ones.

All subzone average maps of Goldwyer II and III do not pass the cut-off conditions, where TOC and PHIT maps generally do not pass their cut-off values. In fact, only small areas of GDWR1a and GDWR1b pass those conditions.

Based on the conditions applied, the resultant maps are only showing the southern flanks in the middle Barbwire Terrace to be prospective in the top two subzones of GDWR1a and GDWR1b (Fig. 16). It is noteworthy that the thickness of those areas for each subzone ranges between 14 and 22 m. The same areas were also the most prospective in the previous approach. However, the potentially prospective areas of the northwest portions of the Barbwire Terrace in the earlier sweet-spot maps are deemed non-prospective here.

Nonetheless, it is essential to note that lateral extensions of prospective areas in the cut-off approach would vary based on the thickness of the subzones. For example, if we treat the Goldwyer section as a whole and produce one average map of each property for the whole formation, no area across the Barbwire Terrace would be considered prospective based on our cut-off conditions. The reason is that the generally thin intervals of prospective shales are masked by the thick non-prospective intervals. On the other hand, if average maps were taken for thinner subzones, those prospective intervals would be more prominent and hence prospective areas would be more laterally extended, while being vertically reduced. This emphasizes some limitations of the average maps and how they should not be analyzed independently. Well data and 3D property models should be incorporated into the assessment process to provide a sufficient shale evaluation.

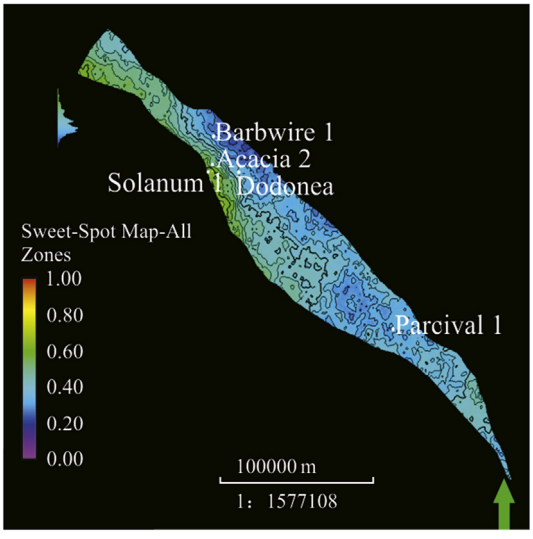

Fig. 15. Sweet-Spot map of the whole Goldwyer Formation in the Barbwire Terrace.

7. Conclusions

This study provided a prospectivity assessment of the Goldwyer Formation as an unconventional resource. This was achieved by sweet-spot mapping through formation evaluation and petrophysical modelling of the shale play. Total organic carbon, total porosity, water saturation, and brittleness index were considered key properties of formation evaluation, and hence were all estimated for wells in the Barbwire Terrace.

Property estimations provided valuable information about the Goldwyer Formation as a potential unconventional resource. Water saturation values have shown to be generally around 30% or less in most non-lean shaly intervals. Brittleness index is quite variable across the Goldwyer, but generally showing values of sufficient brittleness for hydraulic stimulation. Total porosity values range between 0 and 10%, where porosities tend to be lowest in the lean carbonate intervals. Nonetheless, TOC can be considered the most significant property of all four since it has the lowest range of values of less than 2.5%. This low range of TOC can negatively affect the potential of the Goldwyer as a hydrocarbon resource more than any other estimated property. If future wells in the Barbwire Terrace show no improvement in TOC, hydrocarbon production of such intervals may turn out to be non-commercial.

Petrophysical modelling provided a geostatistical distribution of properties in the Barbwire Terrace. The generated models would be improved if more wells were incorporated with better scattering. Furthermore, such geostatistical distribution can be more

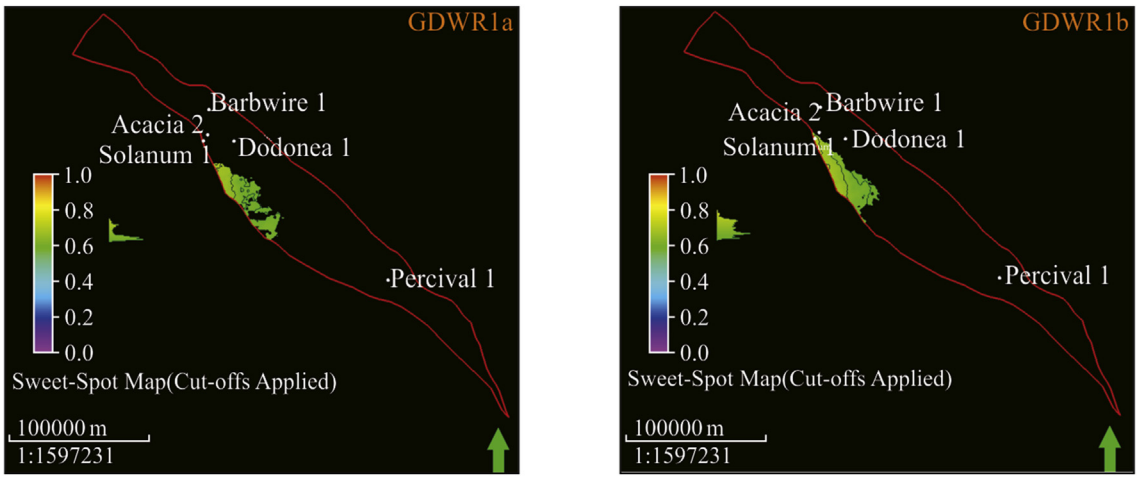

Fig. 16. The southern flanks in the middle Barbwire Terrace in the top two subzones of GDWR1[a] and GDWR1[b].

informative if more data were inputted in the modelling process. For instance, fault models and 3D seismic attributes can uplift data distribution if incorporated in the petrophysical modelling process or even in a surface generation. Although such data were either not available or outside the scope of this study, there is always a room for improvement in any generated model as more data is acquired and interpreted.

The resultant one sweet-spot map generated for the whole Goldwyer provided a broad analysis of the shale play. It highlights the most prospective geographical locations of the Barbwire Terrace which are the southern flanks of the middle and north-western part of the terrace. On the other hand, the generated eleven sweet-spot maps provide a more detailed look into different sections of the Goldwyer Formation, by which most prospective intervals can be identified. Such maps have shown that the top zone (Goldwyer I) is the most prospective zone of all three. Prospective values are the highest in GDWR1b. GDWR1a is a close second, where GDWR3a and GDWR3b come in third and fourth order, respectively. Applying cut-off values for the sweet-spot mapping process provided a more strict analysis of the Goldwyer Formation. Only limited areas of the southern flanks of Barbwire Terrace of GDWR1b and GDWR1a showed prospectivity that have met the cut-off values conditions.

Sweet-spot mapping is a valuable tool that attempts to simplify the complexity of shale play evaluation. The combination of different properties into one map provides a robust assessment of the shale play. Nevertheless, such maps should only be utilized as a reference summary of the assessment and not to replace the comprehensive interpretation of the individual properties. The more data incorporated into a sweet-spot map, the more meaningful it is.

Acknowledgements

We would like to acknowledge Schlumberger for their generous donation of *Petrel* licenses and Saudi Aramco for sponsoring the author's studies at Curtin University.

References

[1] S.J. Cadman, L. Pain, V. Vuckovic, Le Poidevin, S. R, Canning Basin, W.A. Australian petroleum accumulation, department of primary industries and energy bureau of resource sciences, Petroleum Resource Branch (1993). Report 9.
[2] World Shale Gas Resources: an Initial Assessment of 14 Regions outside the United States, 2011 (Retrieved from U.S. Energy Information Administration).
[3] R.R. Towner, D.L. Gibson, Geology of the onshore Canning Basin, western Australia. Bureau of mineral resources, Geology and Geophysics, Australia, Bulletin 215 (1983).
[4] P.W. Haines, Depositional facies and regional correlations of the ordovician goldwyer and nita formations Canning Basin, western Australia with implications for petroleum exploration, Geological Survey of Western Australia (2004). Record 2004/7.
[5] N.E. Triche, M. Bahar, Shale gas Volumetrics of unconventional resource plays in the canning basin, western Australia, in: SPE Unconventional Resources Conference and Exhibition-Asia Pacific, 2013, https://doi.org/10.2118/167078-ms.
[6] S.A. Brown, J.M. Boserio, K.S. Jackson, K.W. Spence, The geological evolution of the Canning Basin: implications for petroleum exploration, in: Paper Presented at the Proceedings of Geological Society of Australia/Petroleum Exploration Society of Australia Symposium, Perth, 1984.
[7] Wapims. Western Australia's petroleum & geothermal information management System. Department of mines and petroleum.
[8] J.W. Schmoker, Use of formation-Density logs to determine organic-carbon content in devonian shales of the western appalachian Basin and an additional example based on the bakken Formation of the williston basin, Petroleum Geology of the Black Shale of Eastern North America (1989).
[9] M.R. Kamali, A.A. Mirshady, Total organic carbon content determined from well logs using ΔLogR and Neuro Fuzzy techniques, J. Petrol. Sci. Eng. 45 (3–4) (2004) 141–148. https://doi.org/10.1016/j.petrol.2004.08.005.
[10] S.Z. Sun, Y. Sun, C. Sun, Z. Liu, N. Dong, Methods of calculating total organic carbon from well logs and its application on Rock's properties analysis. GeoConvention 2013: integration, Geoscience Engineering Partnership (2013).
[11] T.C. Hester, J.W. Schmoker, Determination of Organic Content from Formation-density Logs, Devonian-mississippian Woodford Shale, Anadarko Basin, Oklahoma, 1987 (87–20). Retrieved from http://pubs.er.usgs.gov/publication/ofr8720.
[12] Q.R. Passey, S. Creaney, J.B. Kulla, F.J. Moretti, J.D. Stroud, A practical model for organic richness from porosity and resistivity logs, AAPG (Am. Assoc. Pet. Geol.) Bull. 74 (12) (1990) 1777.
[13] B. Cluff, M. Miller, Logs Evaluation of Gas Shales: a 35-year Perspective, Presentation, DWLS Luncheon, Denver, CO, 2010.
[14] G.E. Archie, The Electrical Resistivity Log as an Aid in Determining Some Reservoir Characteristics, 1942, https://doi.org/10.2118/942054-G.
[15] M. Labani, R. Rezaee, Petrophysical Evaluation of Gas Shale Reservoirs Fundamentals of Gas Shale Reservoirs, John Wiley & Sons, Inc, 2015, pp. 117–137.
[16] C.H. Sondergeld, K.E. Newsham, J.T. Comisky, M.C. Rice, C.S. Rai, Petrophysical considerations in evaluating and producing shale gas resources, in: SPE Unconventional Gas Conference, Pittsburgh, Pennsylvania, 2010, https://doi.org/10.2118/131768-MS.
[17] J.C. Glorioso, A.J. Rattia, unconventional reservoirs: basic petrophysical concepts for shale gas, in: SPE/EAGE European Unconventional Resources Conference and Exhibition, Vienna, Austria, 2012, https://doi.org/10.2118/153004-MS.
[18] G. Yu, R. Aguilera, Use of pickett plots for evaluation of shale gas formations, in: SPE Annual Technical Conference and Exhibition, Denver, Colorado, 2011, https://doi.org/10.2118/146948-MS.

[19] H. Zhao, N.B. Givens, B. Curtis, Thermal maturity of the Barnett Shale determined from well-log analysis, AAPG (Am. Assoc. Pet. Geol.) Bull. 91 (4) (2007) 535–549, https://doi.org/10.1306/10270606060.
[20] D.L. Luffel, F.K. Guidry, New core analysis methods for measuring reservoir rock properties of Devonian Shale, J. Petrol. Technol. 44 (11) (1992) 1184–1190, https://doi.org/10.2118/20571-pa.
[21] D.J. Jacobi, J.J. Breig, B. LeCompte, M. Kopal, G. Hursan, F.E. Mendez, J. Longo, Effective geochemical and geomechanical characterization of shale gas reservoirs from the wellbore environment: caney and the woodford shale, in: SPE Annual Technical Conference and Exhibition, New Orleans, Louisiana, 2009, https://doi.org/10.2118/124231-MS.
[22] R.M. Sneider, J.S. Sneider, G.W. Bolger, J.W. Neasham, Comparison of seal capacity determinations: conventional core vs, Cuttings. AAPG Memoir 67 (1997).
[23] R.K. Olson, M.W. Grigg, Mercury injection capillary pressure (MICP) a useful tool for improved understanding of porosity and matrix permeability distributions in shale reservoirs, in: AAPG Annual Convention, San Antonio, Texas, 2008.
[24] J.A. Franquet, M.W. Bratovich, R.D. Glass, State-of-the-Art openhole shale gas logging, in: SPE Saudi Arabia Section Technical Symposium and Exhibition, Al-khobar, Saudi Arabia, 2012, https://doi.org/10.2118/160862-MS.
[25] F.P. Wang, J.F.W. Gale, Screening criteria for shale-gas systems, Gulf Coast Association of Geological Societies Transactions 59 (2009) 779–793.
[26] D.M. Jarvie, R.J. Hill, T.E. Ruble, R.M. Pollastro, Unconventional shale-gas systems: the Mississippian Barnett Shale of north-central Texas as one model for thermogenic shale-gas assessment, AAPG (Am. Assoc. Pet. Geol.) Bull. 91 (4) (2007) 475–499, https://doi.org/10.1306/12190606068.
[27] W.V. Grieser, J.M. Bray, Identification of production potential in unconventional reservoirs, Production and Operations Symposium (2007) doi:SPE 10.2118/106623-ms.
[28] R. Rickman, M. Mullen, E. Petre, B. Grieser, D. Kundert, A practical use of shale petrophysics for stimulation design optimization: all shale plays are not clones of the Barnett shale, in: SPE Annual Technical Conference and Exhibition, 2008. SPE 115258.
[29] G.A. Waters, R.E. Lewis, D. Bentley, The effect of mechanical properties anisotropy in the generation of hydraulic fractures in organic shales, in: SPE Annual Technical Conference and Exhibition, Denver, Colorado, 2011, https://doi.org/10.2118/146776-MS.
[30] J.P. Castagna, M.L. Batzle, R.L. Eastwood, Relationships between compressional-wave and shear-wave velocities in clastic silicate rocks, Geophysics 50 (4) (1985) 571–581, https://doi.org/10.1190/1.1441933.
[31] A. Royle, S. Bezdan, Shear-wave velocity estimation techniques: a comparison, in: CSEG Convention, 2001.
[32] J. Gonzalez, R. Lewis, J. Hemingway, J. Grau, E. Rylander, R. Schmitt, Determination of formation organic carbon content using a new neutron-induced gamma ray spectroscopy service that directly measures carbon, in: SPWLA 54th Annual Logging Sympsium, 2013.
[33] T. Smithson, How Porosity Is Measured. Oilfield Review, Schlumberger, 2012, pp. 63–64.
[34] J.G. Speight, The Chemistry and Technology of Petroleum, 5 ed., CRC Press, Taylor and Francis, Boca Raton, FL, United States, 2014.
[35] B.P. Tissot, D.H. Welte, Petroleum Formation and Occurrence: a New Approach to Oil and Gas Exploration, Springer-Verlag, New York, 1978.
[36] J.A. Ward, Kerogen density in the marcellus shale, in: SPE Unconventional Gas Conference, 2010. SPE 131767.
[37] D.M. Jarvie, B. Claxton, B. Henk, J. Breyer, Oil and shale gas from the Barnett shale, ft. Worth basin, Texas, AAPG National Convention (2001). Denver, CO June 3-6, 2001.
[38] Glover, P. Petrophysics MSc Course Notes. University of Leeds, UK.
[39] R.C. Selley, Elements of Petroleum Geology, 2 ed., Academic Press, 1998.
[40] I. Clark, Statistics or geostatistics? Sampling error or nugget effect? J. S. Afr. Inst. Min. Metall 110 (2010) 307–312.